

RESEARCH PAPER

Dielectric contrast measurements on biological substances with resonant microwave near-field sensors

NORA HAASE AND ARNE F. JACOB

Resonant substrate integrated near-field sensors are used for characterization of aqueous solutions at three different frequencies. In addition, Chinese hamster ovary (CHO) cells in a culture medium are characterized with the same sensors. Different concentrations as well as different vital states of cell suspensions are examined. The complex permittivity of the samples is evaluated using a linearized method based on perturbation theory. The permittivity differences between the measured cell suspensions are discussed. The resonant frequencies of the sensors are close to 3, 7, and 11 GHz, respectively.

Keywords: Characterization of Material parameters, Medical and biological effects

Received 26 October 2012; Revised 2 April 2013; first published online 10 May 2013

I. INTRODUCTION

In past years, an interest in using microwaves for biomedical imaging and treatment has emerged. The main advantages of microwaves compared to, e.g., X-rays, is the non-ionizing and therefore harmless effect on biological tissues. Several different approaches have been proposed to use microwaves for hyperthermia to improve cancer treatment [1], as sensors for breast cancer imaging [2], and recently in microfluidic devices for permittivity measurements of cell suspensions [3]. The latter is intended as a tool for characterization of biological cells in addition to conventional methods.

The realization of sensing devices capable of analyzing single cells subject to different mechanical or electrical stresses is of great interest [4]. However, in methods used today, including optical [5] sensors, cells have to be treated with specific markers. Using electromagnetic sensors based on low-frequency impedance spectroscopy, several properties of biological cells can be analyzed without such markers [6]. However, since low-frequency methods can only be used in an environment of low conductivity, the cells cannot be examined in a culture medium, since this is always enriched with salts and is therefore conductive.

At higher frequencies, i.e. in the GHz range, the effect of ions in aqueous solutions becomes less and less pronounced, since loss due to conductivity is inversely proportional to frequency. For this reason, sensors in the microwave range may be an interesting alternative for cell analysis in a natural environment.

Several studies on breast cancer tissues have shown a significant permittivity contrast between healthy and diseased samples [7]. A contrast between diseased and cancerous cells has also been shown for single cells at lower frequencies [8]. In this paper, a sensor is introduced which can be used for measurements on cell suspensions in the microwave frequency range. Using micro fabrication and a microfluidic channel, such a system could be downscaled to meet the requirements for single cell measurements.

The proposed sensors are resonant near-field sensors with sensing tips between 30 and 100 micrometers. The sensing volume of such devices is in the order of the sensing tip and depends on the geometry of the ground electrodes surrounding the tip [9]. For this reason, these sensors are restricted to measurements on cell suspensions since the sampling volume is larger than a single cell (diameter 12–16 μm). Using sensors of different size, contrasts of cell suspensions can be evaluated at different frequencies. This gives insight into which frequency bands are most suitable for such measurements and indicates the limits of resonant measurements on highly lossy materials.

The proposed sensors are introduced in Section II. Results of measurements on aqueous solutions and the linearized perturbation approach for the determination of complex permittivity are described in Sections III (A) and III (B), respectively. The permittivity of biological cell suspensions in different concentrations and vital states is recorded and the resulting contrasts are presented in Section IV. The results are summarized in Section V.

II. SENSING DEVICE

Three near-field sensors with resonances close to 3, 7, and 11 GHz are used in the following measurements. The

Institut für Hochfrequenztechnik, Technische Universität Hamburg-Harburg, 21073 Hamburg, Germany. Phone: +49 (0)40-42878-2225

Corresponding author:

Nora Haase

Email: nora.haase@tu-harburg.de

sensors are differently scaled versions of a device proposed in [10]. The structure is based on a twice folded resonator as introduced in [11]. A protruding planar tip connected to the corner of the open edge on the middle layer of the folded structure extends the electrical field maximum onto the tip [12]. The change of resonance when placing a sample in the evanescent fields at the open tip contains the information needed to obtain complex permittivity of the sample, as will be shown in Section III (B). The resulting design is a substrate integrated sensor with low volume due to folding which can be easily integrated with processing electronics.

The resonant cavities of the sensors are fed via two inductive loops. For evaluation of the resonance, the transmission parameter is recorded with a vector network analyzer. The resonant frequency f_r then corresponds to the frequency at which the transmission is maximum and the unloaded (i.e. without the coupling effects) quality factor Q_0 can be extracted using the 3 dB bandwidth and the amplitude of the transmission parameter at maximum [13]. These resonator parameters include the interaction between the sampling tip and sample. In the following, the term 'loaded' is used to describe the coupling of a sample to the sampling tip of the sensing device. This does not refer to a different calculation of the quality factor. The parameters are extracted from the measurement data using Matlab[®].

The geometry of the sensors is sketched in Fig. 1 and the indicated parameters of the three sensors are given in Table 1. The substrate material is Rogers laminate R04003c.

The resolution of microwave near-field sensors has been discussed in the literature [14]. It mainly depends on the geometry of the sensing tip and the (dielectric) contrast of the sample. For conciseness, the resolution related experiments we conducted are not further described here. The results are in agreement with the published results. Generally speaking, the resolution limit is of the order of the tip size, i.e. around

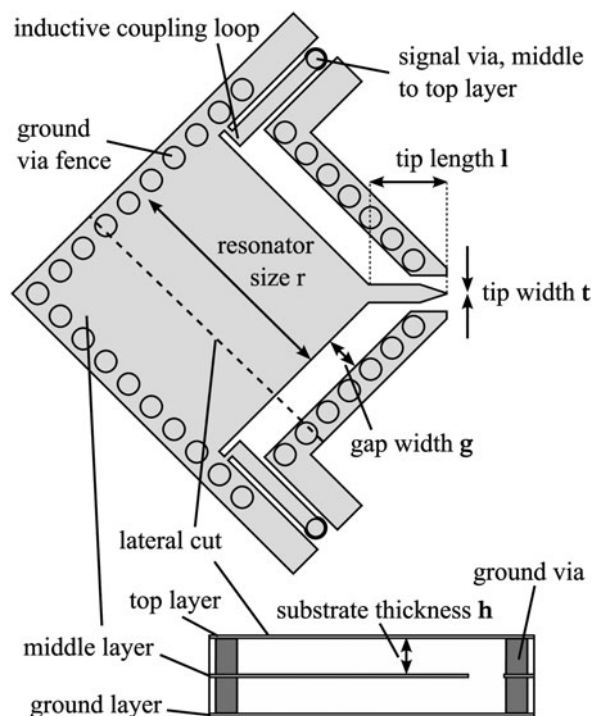


Fig. 1. Sketch of a folded near-field sensor.

Table 1. Geometry parameters of the folded near-field sensors.

	r [mm]	g [mm]	l [mm]	t [μm]	h [mm]	th_m [μm]
Sensor 1	12.7	2	4.3	100	3.1	50
Sensor 2	6.6	0.8	0.9	30	0.8	17
Sensor 3	3.7	0.8	0.9	30	0.8	17

120 μm for Sensor 1 and around 50 μm for the other two sensors. However, with sensors used mainly for determination of a dielectric contrast and not a spatial profile, it is more interesting to discuss the sensitivity limits. In this case, the sensitivity when measuring aqueous solutions is most interesting since many biological media have a high water content.

In addition, the sensor can be calibrated using deionized water and salt solutions of different concentrations, since the permittivity of these liquids is known from the literature [15].

III. MEASUREMENT SETUP

Biological culture media for cell cultivation are usually water-based solutions enriched with salts and carbohydrates as well as with proteins [16]. In order to measure the permittivity of such liquid samples, a closed container is needed. For this purpose a funnel milled into a Plexiglas[®] plate is fixed on top of the sensing tip. A sketch of the measurement setup is given in Fig. 2 with the geometry of the funnel. The volume of the funnel is approximately 0.1 ml. The resonant frequencies and quality factors of the sensors loaded with air are presented in Table 2.

A) Aqueous solutions

In order to perform measurements on samples similar to a biological cell suspension, household salt (mainly sodium chloride) and sugar (mainly sucrose) are dissolved in deionized water in different concentrations. The concentrations are given in % w/w. The samples are then filled into the funnels and the resulting resonances are recorded.

Figure 3 shows the resonant frequency versus quality factor for the three sensors. The changes of resonance caused by the salt solutions (green stars) are similar for all sensors. Increasing the concentration mainly affects the quality factor and to a lower degree also the resonant frequency.

It is worth noting that an increasing salt concentration, i.e. conductivity, has a greater impact on sensors with lower resonant frequency. This is expected since the effect of conductivity on permittivity decreases with frequency. The effect of dissolved sugar (red plus signs) also differs for the sensors, especially regarding the quality factor. The resonant frequency increases for all sensors, while the quality factor decreases for Sensor 1 but increases for Sensor 3. The quality factor of Sensor 2 is hardly affected. This indicates, at least for higher frequencies, that the dissolved sugar, a non-ionic but slightly polar molecule, reduces permittivity and even loss of the solution. These results are in agreement with measurements on sucrose solutions performed by Kent in similar frequency ranges [17].

In order to estimate reproducibility, each solution is measured several times. A new sample is used in each measurement, i.e. the funnel is emptied and refilled between all measurements. The plots show the average values for each solution.

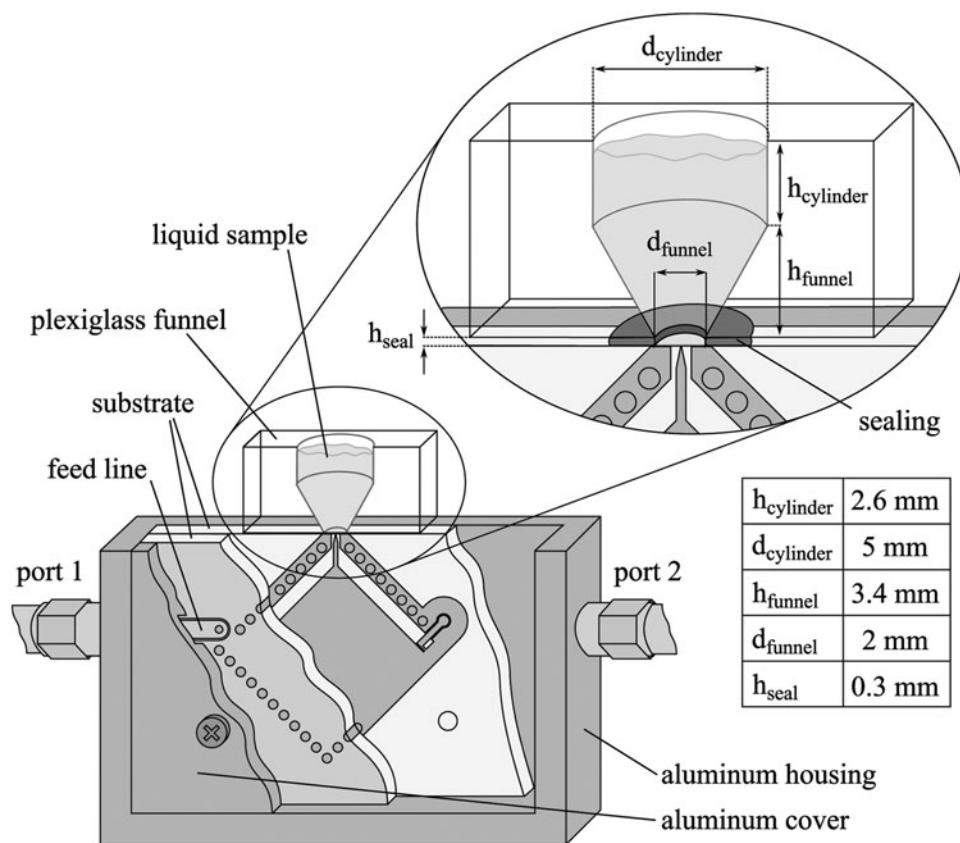


Fig. 2. Measurement setup for liquid samples using substrate integrated sensor.

The error sources in this setup can be separated into three different groups.

The first error source is the electrical noise inherent to the network analyzer. Secondly, the solutions themselves may not be perfectly homogeneous, so that the samples can be slightly different from each other. This can be seen as a chemical error. Thirdly, the funnel structure is not perfectly sealed and the surface is not perfectly smooth. The elastic rubber seal may allow for some of the liquid to creep into the small gaps at the junctions of different materials and surface roughness can hinder wetting of the surface around the sensing tip. The resulting errors are thus due to mechanical inaccuracies.

The three error sources can be evaluated by the recorded resonator parameters for the sample air, water, and saline solutions. The encountered standard deviations for Sensor 1 are given in Table 3. For air samples, the only error that can occur is the electrical noise since the other two error sources do not apply here. The deviation of resonant frequency is lower than numerical accuracy used in the evaluation. The standard deviation of the quality factor is also very low (0.1%). For the water samples, the mechanical inaccuracies also play a role, but not the chemical ones, since deionized water is homogeneous. As can be seen in Table 3, the deviations are

significantly larger for water samples compared to air. It is obvious that the electrical noise is small compared to the mechanical inaccuracies. The saline solutions also include chemical inaccuracies. However, the encountered deviations are lower than water samples. This indicates that the chemical inaccuracies are also negligible, which is expected at concentrations much lower than in a saturated solution.

The measured resonances show that the sensors can discriminate between different concentrations. The salt concentration is most easily determined at lower frequencies because of the higher influence of ions on permittivity. The sugar solutions can be discriminated best at higher frequencies because of strong influence on resonant frequency.

All in all, the quality factors are drastically lower when measuring aqueous solutions than with an air sample (compare Table 2). This is caused by high losses of water at microwave frequencies and by strong coupling between the sensor and the sample which is necessary for high sensitivity. The loss tangent of water according to the well established Debye model increases by up to almost 2 in the higher GHz range [18]. Therefore, resonant sensors such as these may be less suitable for measurements on biological substances at even higher frequencies since the quality factor of the sensors will be extremely low leading to difficulties in evaluation of the resonance.

Table 2. Resonator parameters of the sensors loaded with air.

	Sensor 1	Sensor 2	Sensor 3
$f_{r,o}$ (GHz)	3.32	7.32	11.14
Q_o	116.9	184.5	129.7

B) Evaluation based on perturbation theory

In order to obtain quantitative results for measured permittivity, a perturbation approach is chosen. The change of

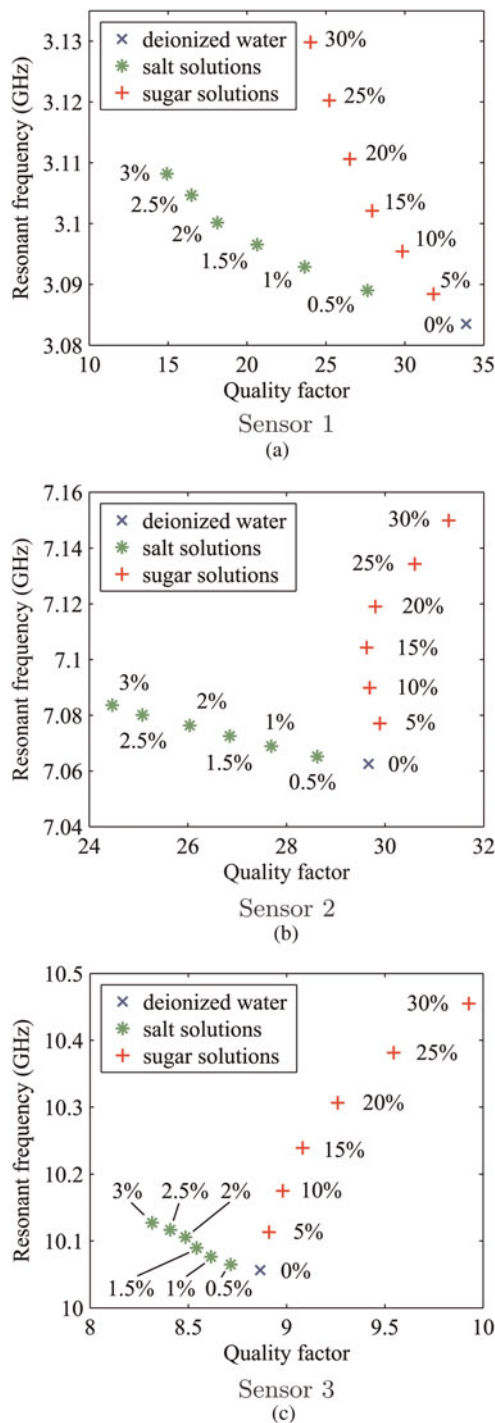


Fig. 3. Measured resonator parameters for different aqueous solutions.

Table 3. Standard deviations of resonant frequencies and quality factors encountered in measurements with air, water, and saline solution samples with Sensor 1 for error discussion.

	Air	Water	Saline
$\Delta f_{r,o}$ (MHz)	0	1.3	1.1
$\Delta Q_o/Q_o$ (%)	0.1	1.1	0.6

resonance of microwave near-field sensors can be described by perturbation theory because field changes occur only in the small sampling volume at the tip. The frequency shift of a dielectric (non-magnetic) perturbation, in this case the sample with a relative permittivity ϵ_r , is given by [19]

$$\frac{f_1 - f_0}{f_0} \approx - \frac{\iiint_{V_s} \epsilon_o(\epsilon_{r1} - \epsilon_{r0})E_1E_o^*dV}{\iiint_{V_{res}} \epsilon|E_o|^2 + \mu|H_o|^2dV}, \tag{1}$$

where V_s is the sampling volume of the sensor and V_{res} is the total resonator volume. The subscripts 0 and 1 of frequency f , relative permittivity ϵ_r , and electric field vector E refer to the unperturbed and the perturbed scenario, respectively. The material inside the resonator has permittivity $\epsilon = \epsilon_o\epsilon_{r,res}$ and permeability $\mu = \mu_o\mu_{r,res}$.

Since the permittivity of aqueous solutions and cell suspensions is close to that of water, some approximations can be made. First, for a homogeneous sample relative permittivity can be pulled out from the integral. Second, since the permittivity changes only slightly, the perturbed electrical field E_1 can be assumed to be equal for all aqueous samples. The unperturbed sensor refers to an empty funnel, i.e. $\epsilon_{r0} = 1$ (air). The reference permittivity of water $\epsilon_{r1} = \epsilon_{r,water}(f_r)$ for the integral can be calculated from the Debye model

$$\epsilon_{r,water}(f) = \epsilon_{\infty,water} + \frac{\epsilon_{o,water} - \epsilon_{\infty,water}}{1 - j2\pi\tau_{water}f} \tag{2}$$

for each sensor at the respective resonant frequency. The static and high-frequency permittivities $\epsilon_{o,water}$ and $\epsilon_{\infty,water}$ as well as the relaxation time τ_{water} in equation (2) are determined using the equations developed in [15] at 20°C. The volume integral over the electric and magnetic energy in the sensor

$$\frac{\iiint_{V_s} \epsilon_oE_{water}E_o^*dV}{\iiint_{V_{res}} \epsilon|E_o|^2 + \mu|H_o|^2dV} = \frac{f_o - f_{water}}{f_o(\epsilon_{r,water} - 1)} = C \tag{3}$$

is assumed to be equal for different aqueous samples.

In equation (3), the resonant frequency can be substituted by the equivalent complex resonant frequency [20]

$$f_{cr,i} = f_{r,i} \left(1 + j \frac{1}{2Q_{o,i}} \right). \tag{4}$$

Here, subscript i refers to the sample in the funnel, i.e. air, water, etc.

Using the complex permittivities and resonant frequencies of air and water, C can be calculated from equation (3). The complex resonant frequencies of air and water and the resulting complex C s are listed in Table 4. The complex permittivity $\epsilon_{r,s}$ of a sample loaded in the funnel is obtained from

$$\epsilon_{r,s} = \epsilon'_{r,s} - j\epsilon''_{r,s} = \frac{f_{c,o} - f_{c,s}}{f_{c,o}C} + 1, \tag{5}$$

with $f_{c,s}$ the measured complex resonant frequency of the sensor. In the following, the real part of complex permittivity

Table 4. Complex resonant frequencies and constants C used in the perturbation approach for calculation of complex permittivity.

	Sensor 1	Sensor 2	Sensor 3
$f_{r,c,air}$	$3.3171 + j0.0142$	$7.3240 + j0.0198$	$11.1401 + j0.0430$
$f_{r,c,water}$	$3.0804 + j0.0481$	$7.0626 + j0.1190$	$10.0565 + j0.5672$
C	$(92.6 + j2.06)10^{-5}$	$(52.2 + j0.252)10^{-5}$	$(158 + j7.41)10^{-5}$

ϵ_r' will be referred to as permittivity and the imaginary part ϵ_r'' as loss factor.

The frequency dependent complex permittivity of deionized water and saline solutions is well known from the literature. The values given in the following refer to the results of Stogryn in [15].

The accuracy of the approach is estimated by comparing the calculated and the reference permittivities. The values from the measurement and the literature are shown in Fig. 4. Obviously, the accuracy of the approximation decreases for higher salt concentrations. However, for salt concentrations below 1%, the deviation to the reference value is lower than 3% for all sensors except Sensor 1, for which the error is higher (5.4%) for the loss. The reason for this is the large change of the loss at 3 GHz due to increased conductivity. When increasing the conductivity, the field distribution changes slightly compared to the case with a water sample. Thus, the assumptions made in equation (3) become less accurate, which leads to some error.

Previous measurements on cell suspensions have shown that permittivity in the frequency range considered here is quite close to that of water, while the loss is decreased by a factor of up to two [21]. This is similar to the contrast encountered in the measurement on saline solutions with Sensor 1, where the loss is increased by more than a factor two. Even though the error is not negligible, an evaluation such as this can thus yield a decent estimation of permittivity of cell suspensions. The permittivity estimations for cell suspensions examined in the following can be expected to be within approximately 5 and 10% of the true value for the real and the imaginary part, respectively.

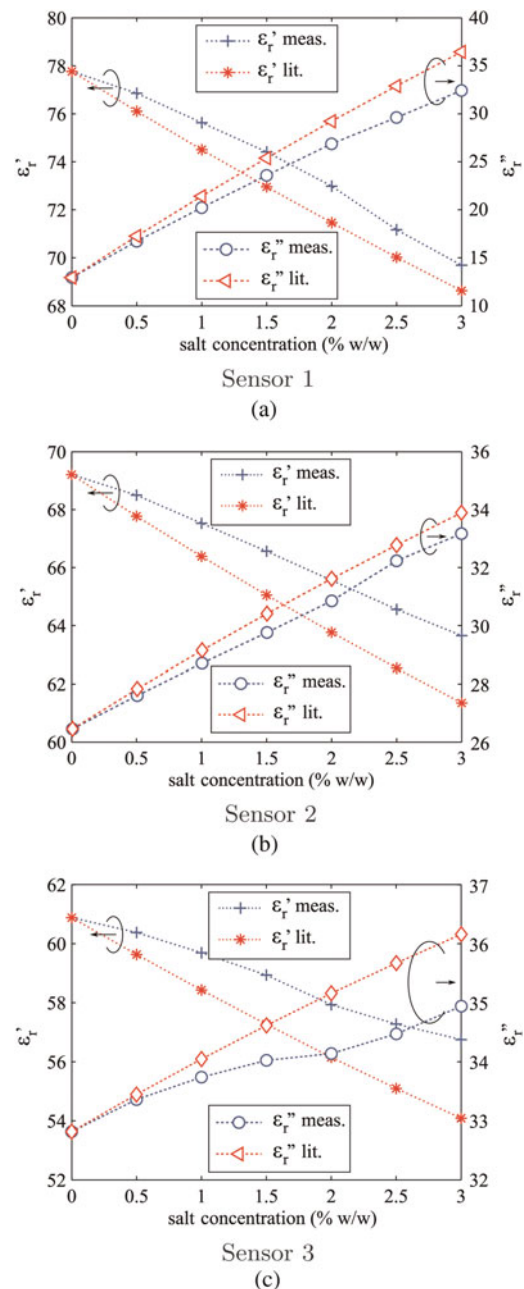
However, since the slope of the calculated permittivity for saline solutions is quite similar to the reference (see Fig. 4), small dielectric contrasts can still be determined with this method since the errors due to the perturbation approach essentially cancel each other.

IV. BIOLOGICAL MEASUREMENTS

The permittivity of cell suspensions is determined using the perturbation approach introduced in Section III (B). Deionized water at room temperature (20°C) is once more used as reference material. The two different experiments performed are described below.

The Chinese hamster ovary (CHO) cells used in the experiments are cultivated at the Institute of Bioprocess and Biosystems Engineering at Technische Universität Hamburg-Harburg. The culture medium used is TeutoCell AG TC-42 which is enriched with 4mM Glutamine before cultivation. The diameter of CHO cells varies between 12 and 16 μm .

Prior to the experiments comparing different cell suspensions, the reproducibility of response of sedimenting CHO

**Fig. 4.** Measured and reference [15] permittivity values for different saline solutions.

cells has to be verified. For this purpose, a cell suspension with 5×10^6 cells/ml medium is tested several times with samples from different batches of cells. The results for Sensor 1 are shown in Fig. 5. The reproducibility of resonant frequency is very good. The average frequency shift is 16.5 MHz with a standard deviation of 0.96 MHz. The

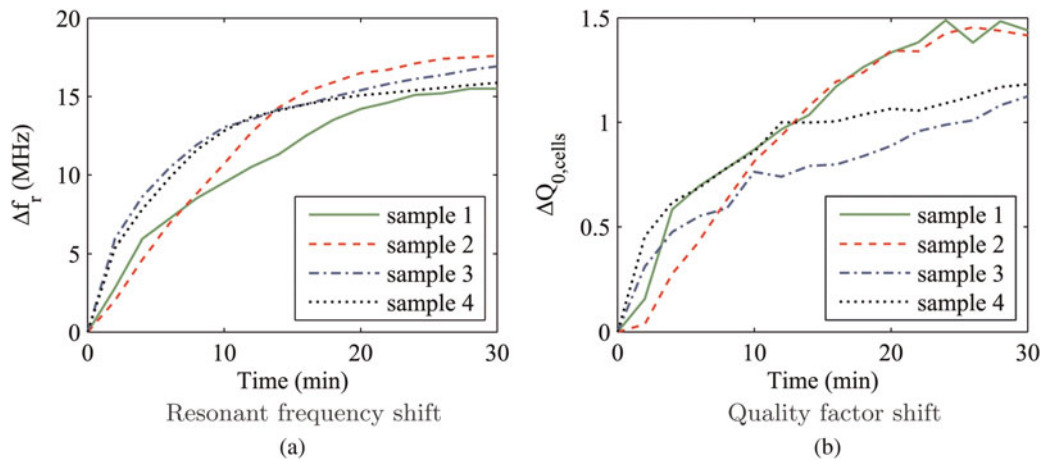


Fig. 5. Reproducibility test with cell suspensions of different cultivation batches.

mean shift in quality factor is 1.2 with a standard deviation of 0.16.

A) Different cell concentrations

In a first measurement, living CHO cells in the culture medium are used in the measurement. The following biological protocol was applied to the cells before the experiments. The cell concentration after cultivation is determined using a hemocytometer and trypan blue. The cells are then separated from the used culture medium with a centrifuge and are resuspended in fresh culture medium to obtain the desired concentration. This is performed for each cell concentration. The protocol is schematically described in Fig. 6.

Three different concentrations, namely $c_1 = 5 \times 10^6$, $c_2 = 10 \times 10^6$, and $c_3 = 15 \times 10^6$ cells/ml culture medium are inserted into the funnels of the sensors successively. Each sample is measured for 30 minutes in order to allow the cells to sediment at the bottom of the funnel, i.e. on the sensing tip as shown in Fig. 7. The thickness h_s of the sedimented cell layer depends on the cell concentration, i.e. it is higher for larger concentrations. Assuming spherical cells with an average radius of $7 \mu\text{m}$ and a dense packing of 74% density, the thickness of the sedimented cell layer can be estimated using geometrical considerations. Assuming that 90% of the funnel volume is filled, the volume of the cell suspension is approximately $80 \mu\text{l}$. The estimated resulting thickness h_s is given in Table 5 for the three concentrations.

The change of resonance resulting from the sedimenting cells is recorded in intervals of 2 minutes. The results are used to calculate the complex permittivity and are depicted exemplarily in Fig. 8 for Sensors 1 and 2. Both permittivity and loss factor of cell suspension decrease during the experiment. This can be explained by the increased volume percent of cells in the sampling volume which have many components than lower permittivity and loss compared to pure water, such as cell membrane, proteins, organelles, etc. The three concentrations can be distinguished with Sensor 1 but not with the other sensors. The reason for this is the smaller sampling volume of Sensors 2 and 3 which is due to the smaller tip size (see Table 1). The main difference between the three cell suspensions is the layer thickness h_s of the sedimented cells. For Sensor 1, apparently, the sampling volume is higher than h_s since a difference between the suspensions can be observed. For the other sensors, the sampling volume is already filled with the sedimented cells in the suspension with 5×10^6 cells/ml, therefore the increased h_s of the other suspensions does not influence the sensors.

The permittivity and loss factor of the sedimented cells, $\bar{\epsilon}'_{r, sed}$ and $\bar{\epsilon}''_{r, sed}$, as well as the dielectric change during sedimentation $\Delta \bar{\epsilon}'_{r, sed}$ and $\Delta \bar{\epsilon}''_{r, sed}$ are summarized in Table 6 for $c = 10 \times 10^6$ cells/ml.

The permittivity of the cell solutions remains below that of water. This is expected because both ionic and non-ionic solvents in the culture medium reduce the permittivity of the liquid as was shown in the experiments with the aqueous

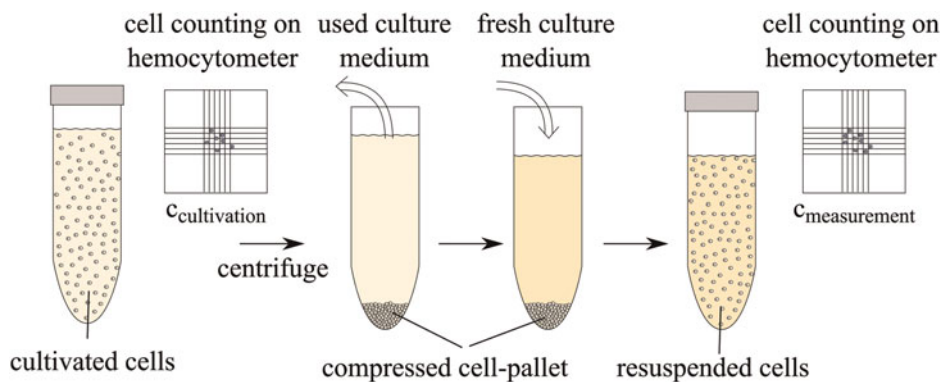


Fig. 6. Biological protocol for preparation of different cell concentrations after cultivation.

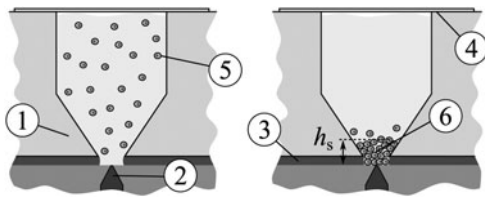


Fig. 7. Sketch of cell behavior in funnel, not to scale. ① Plexiglas funnel, ② sensing tip, ③ seal to prevent leakage, ④ seal to avoid evaporation, ⑤ cells, evenly distributed, ⑥ cells, sedimented.

Table 5. Estimated thickness of sedimented cells based on geometrical considerations.

	C_1	C_2	C_3
h_s	0.25 mm	0.48 mm	0.68 mm

solutions (see Fig. 3). The cells also lower the permittivity, as discussed above. The loss factor is lowered by the sedimenting cells, and this effect increases with frequency because the impact of the ions on dissipation decreases.

B) Different vital states

In a second measurement, the dielectric signature of dead cells is investigated. A cell suspension with concentration $c_2 = 10 \times 10^6$ cells/ml is prepared using the same protocol as mentioned above. Three samples are taken from the cultivated cells and two of them are ‘killed’ in different ways: one cell suspension is shock-frozen and one is treated with mild heat. The biological protocol is sketched in Fig. 9. Sample 1 contains living cells. Sample 2 is immersed into liquid nitrogen at -196°C . As a result of such a temperature shock, ice crystals form inside the cells and the culture medium and as a result the cell membranes burst [22]. Thus, after thawing, the cytoplasm of the cells mixes with the culture medium and the remains of the cell membrane and organelles are distributed in the liquid. Sample 3, heated for 10 minutes at 70°C in a thermoshaker, contains dead cells which are still mainly intact, i.e. the cell membrane is not destroyed in this process. The proteins are merely denatured in the heating process which leads to an immediate cell death [23].

In order to confirm the vital states of the cells, samples of the three cell suspensions are mixed with the vital stain trypan blue. Although the living cells are not colored, dead cells are dyed in dark blue. Photographs taken through a microscope showing the cell suspensions are displayed in Fig. 10. The cells killed with heat are clearly dead but otherwise intact, as expected. In the cell suspension which was shock-frozen, some cells remain alive and some are dead. However, the observed cell concentration is lower in this suspension, since the cells that burst during the frost-thaw cycle are not dyed by the vital stain and are thus not visible.

Prior to the measurements, the cell suspensions are allowed to cool or re-heat to room temperature (20°C), respectively. The different cell suspensions are then filled into the funnels one after the other to sediment on the sensors. The resulting permittivities are shown in Fig. 11 for Sensors 1 and 3. Obviously, the difference between the suspensions affects the loss factor and to a smaller degree also the permittivity.

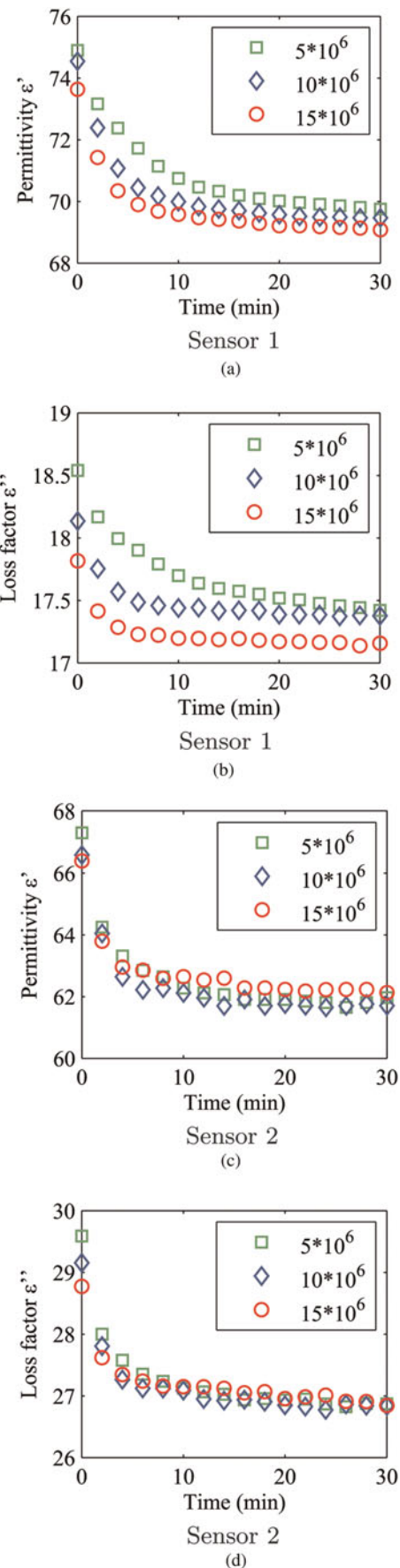


Fig. 8. Complex permittivity of alive cells sedimenting on Sensors 1 and 2 in different concentrations.

Table 6. Permittivity and loss factor of sedimented cells and dielectric change during sedimentation in a cell suspension of $c = 10 \times 10^6$ cells/ml.

	Sensor 1	Sensor 2	Sensor 3
$\bar{\epsilon}'_{r, sed}$	69.47	61.70	54.89
$\bar{\epsilon}''_{r, sed}$	17.38	26.83	34.51
$\Delta\bar{\epsilon}'_{r, sed}$	5.08	4.88	5.73
$\Delta\bar{\epsilon}''_{r, sed}$	0.76	2.32	2.76

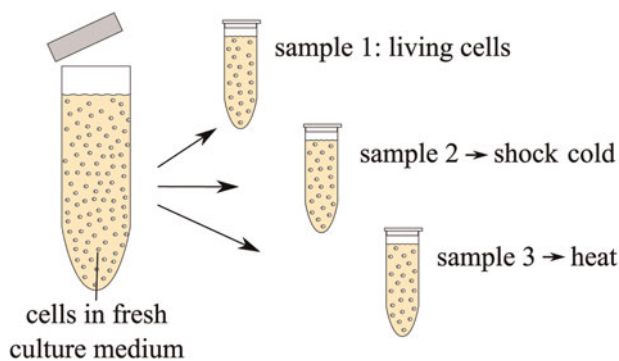


Fig. 9. Biological protocol for preparation of different vital states of cells.

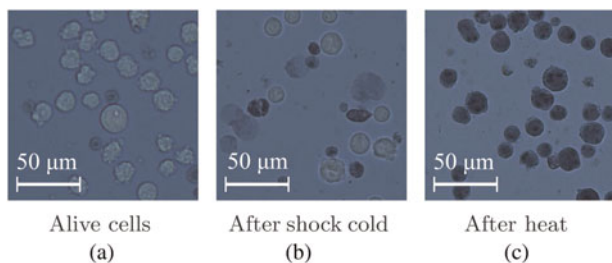


Fig. 10. Images of different vital states of CHO cell suspensions. The colouring indicates the vital state of the cells: light cells are alive, dark cells are dead. Cell fragments are not coloured, therefore not visible optically.

The loss factor of the dead cells is lower than that of the living ones; the values of the frozen cells is between the two other solutions, since both living and dead cells are present in that suspension. This behavior is visible at all three frequencies. The differences $\Delta\epsilon_{r, dead}$ between the permittivity of sedimented living and dead (heated) cells are listed in Table 7.

The measurements show that the dielectric contrast between living and dead cells is significant. Especially the loss factor can be used to discriminate between different cell suspensions used here. In addition, the experimental results are in agreement with optical observations of the cell suspensions concerning the vitality of the cells in the suspensions. In other measurements in the microwave range with living and dead human umbilical vein endothelial cells, similar observations were made concerning the loss factor of the suspension [24], i.e. a lowering of the loss factor for dead cells compared to living ones. In that publication, an increase of the permittivity was found for the dead cells, which is not observed here. However, since the cell suspension investigated here is not the same, the diverging observations are most likely found in biological differences between the cell types.

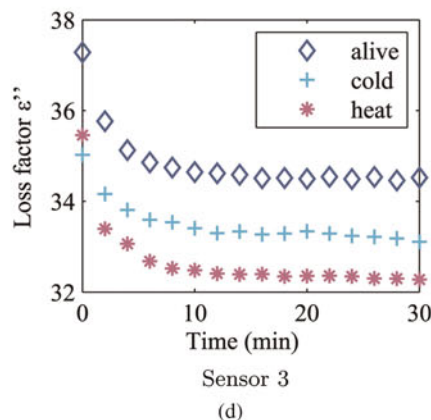
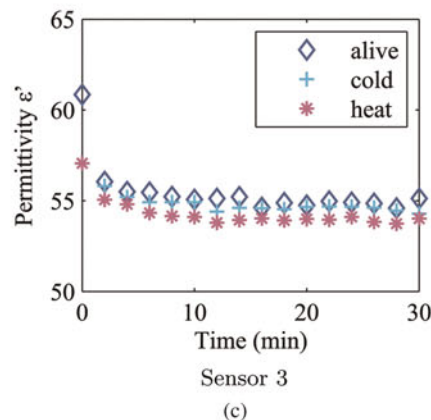
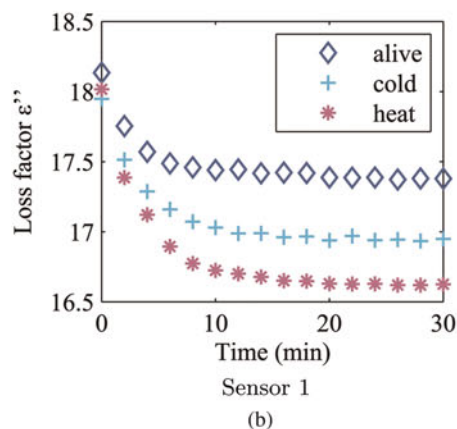
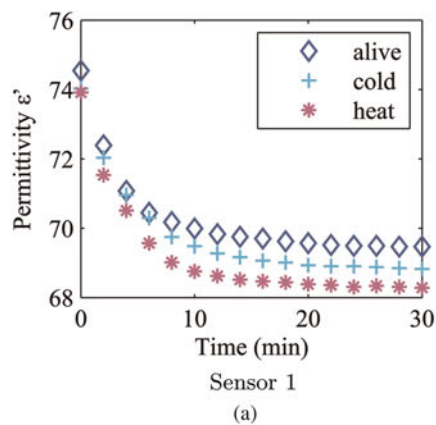


Fig. 11. Calculated complex permittivity of cell sedimentation using Sensors 1 and 3. The cell concentration is 10×10^6 .

Table 7. Difference between permittivity of living and dead cells observed with the sensors.

	Sensor 1	Sensor 2	Sensor 3
$\Delta \epsilon'_{r,dead}$	1.17	0.51	0.96
$\Delta \epsilon''_{r,dead}$	0.76	0.77	2.19

V. CONCLUSION

Substrate integrated near-field sensors for three different resonant frequencies are proposed. They are tested on their ability to characterize aqueous solutions in different concentrations. Using the complex resonant frequency and a linearized perturbation integral, the complex permittivity of the samples is calculated. The accuracy of both the measurements themselves and the evaluation of the recorded resonances is discussed.

Finally, measurements on CHO cells are performed. The contrast between evenly distributed and sedimented cells is significant. Different vital states of cells are also measured, i.e. living cells are compared to dead ones. The experiments yield a distinct contrast. At higher frequencies, the loss factor seems especially promising for discrimination since observed contrast is largest there.

ACKNOWLEDGEMENTS

The authors thank M.Sc. Janina Bahnmann and Prof. Dr rer. nat. An-Ping Zeng from the Institute of Bioprocess and Biosystems Engineering at Technische Universität Hamburg-Harburg for contributing the cultivated CHO cells for the measurements as well as many stimulating discussions concerning the biological context.

REFERENCES

- [1] Sterzer, F.: Microwave medical devices. *IEEE Microw. Mag.*, **3** (2002), 65–70.
- [2] Fear, E.C.; Stuchly, M.A.: Microwave detection of breast cancer. *IEEE Trans. Microw. Theory Tech.*, **48** (2000), 1854–1863.
- [3] Grenier, K.; et al.: New broadband and contact less RF/microfluidic sensor dedicated to bioengineering, in *IEEE MTT-S Int. Microwave Symp. Digest*, (MTT '09). 2009.
- [4] Di Carlo, D.; Lee, L.P.: Dynamic single-cell analysis for quantitative biology. *Anal. Chem.*, **78** (2006), 7918–7925.
- [5] Fu, A.Y.; Spence, C.; Scherer, A.; Arnold, F.H.; Quake, S.R.: A micro-fabricated fluorescence-activated cell sorter. *Nat. Biotechnol.*, **17** (1999), 1109–1111.
- [6] Morgan, H.; Sun, T.; Holmes, D.; Gawad, S.; Green, N.G.: Single cell dielectric spectroscopy. *J. Appl. Phys.*, **40** (2006), 61–70.
- [7] Lazebnik, M.; et al.: A large-scale study of the ultrawideband microwave dielectric properties of normal, benign and malignant breast tissues obtained from cancer surgeries. *Phys. Med. Biol.*, **52** (2007), 6093–6115.
- [8] Cho, Y.; Kim, H.S.; Frazier, A.B.; Chen, Z.G.; Shin, D.M.; Han, A.: Whole-cell impedance analysis for highly and poorly metastatic cancer cells. *J. of Microelectromech. Syst.*, **18** (2009), 808–817.

- [9] Talanov, V.V.; Scherz, A.; Moreland, R.L.; Schwartz, A.R.: A near-field scanned microwave probe for spatially localized electrical metrology. *Appl. Phys. Lett.*, **88** (2006), 134106–(p3).
- [10] Ambroziewicz, M.; Jacob, A.F.: Substrate integrated resonant near-field sensor for material characterization, in *IEEE MTT-S Int. Microwave Symp. Digest (MTT)*, 2010, 23–28 May 2010, 628–631.
- [11] Jia-Sheng Hong.: Compact folded-waveguide resonators. in *IEEE MTT-S Int., Microw. Symp. Dig.*, 2004 vol. 1 (2004), 213–216.
- [12] Haase, N.; Jacob, A.F.: Characterization of biological substances using a substrate integrated microwave near-field sensor. *42nd European, Microwave Conf. (EuMC)*, 2012, October 29–November 1 2012, 432–435.
- [13] Kajfez, D.; Chebolu, S.; Abdul-Gaffoor, M.R.; Kishk, A.A.: Uncertainty analysis of the transmission-type measurement of Q-factor. *IEEE Trans. Microw. Theory Tech.*, **47** (1999), 367–371.
- [14] Gao, C.; Tao, W.; Duewer, F.; Lu, Y.; Xiang, X.-D.: High spatial resolution quantitative microwave impedance microscopy by a scanning tip microwave near-field microscope. *Appl Phys Lett.*, **71** (1997), 1872–1874.
- [15] Stogryn, A.: Equations for calculating the dielectric constant of saline water. *IEEE Trans. Microw. Theory Tech.*, **19** (1971), 733–736.
- [16] Birch, J.R. (1976) United States Patent 4,038,139. High Wycombe, England.
- [17] Kent, M.; Kress-Rogers, E.: The COST 90bis collaborative work on the dielectric properties of foods. In *Physical properties of foods / 2. COST 90bis Final Seminar proceedings*, Elsevier Applied Science, London, (1987), 371–374.
- [18] Kaatz, U.: Complex permittivity of water as a function of frequency and temperature. *J. Chem. Eng. Data*, **34** (1989), 371–374.
- [19] Pozar, D.M.: *Microwave Engineering*, 3rd ed. John Wiley & Sons, New York, Inc., 2005.
- [20] Collin, R.E.: *Foundations for Microwave Engineering*. McGraw-Hill, New Jersey, Inc., 1966.
- [21] Grenier, K.; Dubuc, D.; Poupot, M.; Fournie, J.-J.: Microwave signatures of alive B- lymphoma cells suspensions. in *IEEE Topical Conf. on, Biomedical Wireless Technologies, Networks, and Sensing Systems (BioWireless)*. 2011, 16–19 January 2011, 95–98.
- [22] Mazur, P.: Freezing of living cells: mechanisms and implications. *Am. J. Physiol.*, **247** (1984) C125–C142.
- [23] Henle, K.J.; Dethlefsen, L.A.: Time-temperature relationships for heat-induced killing of mammalian cells. *Ann. New York Acad. Sci.*, **335** (1980) 234253.
- [24] Grenier, K.; Dubuc, D.; Poleni, P.-E.; Kumemura, M.; Toshiyoshi, H.; Fujii, T.; Fujita, H.: Resonant based microwave biosensor for biological cells discrimination. *IEEE Radio and Wireless Symposium (RWS)*, 2010, 10–14 January 2010, 523, 526.



Nora Haase received her Dipl.-Ing. degree in Electrical Engineering at Technische Universität Hamburg-Harburg, Hamburg, Germany in 2011. She is currently working toward her Ph.D. at the Institut für Hochfrequenztechnik at Technische Universität Hamburg-Harburg, Hamburg, Germany, in the field of electromagnetic interaction with biological tissues.

Her research interests include permittivity measurements of biological materials using resonant as well as broadband sensing devices.



Arne F. Jacob received the Dipl.-Ing. degree in Electrical Engineering in 1979 and the Dr.-Ing. degree in 1986 from Technische Universität Braunschweig, Germany. From 1986 to 1988 he was a Fellow at CERN, the European Organization for Nuclear Research, Geneva, Switzerland. In 1988, he joined Lawrence Berkeley Laboratory, University of California at Berkeley and served for almost 3 years

as a Staff Scientist at the Accelerator and Fusion Research Division. In 1990, he became a professor at the Institut für Hochfrequenztechnik, Technische Universität Braunschweig. Since October 2004, he has been a professor at Technische Universität Hamburg-Harburg, Hamburg, Germany, where he heads the Institut für Hochfrequenztechnik. His current research interests include the design, packaging, and application of integrated (sub) systems up to millimeter frequencies, and the characterization of complex materials.